ADVANCED MATERIALS INTERFACES

www.advmatinterfaces.de

# Anisotropic Raman-Enhancement Effect on Single-Walled Carbon Nanotube Arrays

*Juanxia Wu, Shuchen Zhang, Dewu Lin, Bangjun Ma, Liangwei Yang, Shuqing Zhang, Lixing Kang, Nannan Mao, Na Zhang, Lianming Tong,* and Jin Zhang**

**The charge transfer between molecules and materials can modulate the polarizability tensor of the molecules and lead to an enhancement of the Raman scattering. Surface-enhanced Raman scattering on in-plane anisotropic layered materials has suggested the crystalline-axis-dependent charge interactions between molecules and materials. However, the full understanding of the anisotropic charge transfer process is still lacking. The rigorous anisotropic nature and structural diversity of single-walled carbon nanotube (SWNT) provide an ideal platform to systematically study the anisotropic charge transfer process. The present work reports the anisotropic Raman enhancement effect of molecules on horizontally aligned SWNT arrays and attribute it to the charge transfer efficiency that depends on the laser polarization direction and the resonance of SWNTs. The Raman signal of probe molecules on SWNT arrays is enhanced and reaches the maximum intensity when the incident laser is polarized along the SWNT axial direction, and the intensity is the minimum if they are perpendicular to each other. The different efficiencies of charge transfer are further confirmed by polarized optical absorption measurements and the energy alignment analysis. The present work provides a sensitive way to study the tunable charge interactions between molecules and anisotropic low-dimensional materials, which are also important for polarization-controlled optoelectronic applications.**

## 1. Introduction

Raman enhancement on 2D layered materials (graphene, h-BN, $MoS_2$, GaSe, etc.) provides a perfect platform to investigate the pure chemical mechanism (CM) in surface-enhanced Raman scattering (SERS), which concerns the charge interactions involving the electron–photon and electron–phonon interactions between molecules and the 2D materials.[1] In graphene-enhanced Raman scattering (GERS), the enhancement mechanism is attributed to the charge transfer between graphene and molecules, and a number of key factors in the chemical enhancement have been studied, including the first layer effect,[2] the energy band alignment,[3] and the orientation and structural symmetry of probe molecules.[1d,4] Both theoretical and experimental studies have suggested that the maximum enhancement can be obtained when the excitation energy of the incident laser matches the energy difference between Fermi level of graphene and highest occupied molecular orbital (HOMO)/lowest unoccupied molecular orbital (LUMO) level of molecule.[3,5] Different from GERS, strong interfacial dipole–dipole interactions also induce a significant Raman enhancement on h-BN, while both the charge transfer and dipole–dipole interaction take effects in the Raman enhancement on $MX_2$ (M = Mo, W; X = S, Se).[1b,6] Besides, the van der Waals heterostructure of stacking monolayer $WSe_2$ and graphene has shown a larger Raman enhancement factor than that of isolated layers due to that the electronic density of state in graphene was changed by $WSe_2$ through the interlayer coupling.[7]

Recently, anisotropic Raman enhancement effect on 2D materials with lower symmetry, such as orthorhombic black phosphorus (BP) and triclinic rhenium disulfide ($ReS_2$), has been studied, and the anisotropic charge interaction between anisotropic 2D materials and molecules was proposed to explain the angle dependence of the Raman enhancement effect.[8] Although many theoretical and experimental studies have focused on the chemical mechanism of SERS on 2D materials and semiconductor quantum dots,[9] a full understanding of the charge interaction between anisotropic substrates and molecules has not yet been comprehensively investigated. For example, BP and $ReS_2$ are both biaxial crystal, the existence of birefringence effect results in changes in the propagation speed and polarization direction of light within them.[10] Therefore, the anisotropic optical absorption and birefringence effect are difficult to take into account at the same time when the charge interaction between anisotropic 2D materials and molecules are investigated using

J. Wu, S. Zhang, D. Lin, B. Ma, L. Yang, S. Zhang, L. Kang, N. Mao, N. Zhang, Prof. L. Tong, Prof. J. Zhang
Center for Nanochemistry
Beijing National Laboratory for Molecular Sciences
Key Laboratory for the Physics and Chemistry of Nanodevices
State Key Laboratory for Structural
Chemistry of Unstable and Stable Species
College of Chemistry and Molecular Engineering
Peking University
Beijing 100871, P. R. China
E-mail: tonglm@pku.edu.cn; jinzhang@pku.edu.cn

**DOI: 10.1002/admi.201700941**

 

polarized Raman spectroscopy. Therefore, a kind of materials which have a strictly anisotropic structure and relatively simple optical properties will be helpful to systematically study the charge interaction between anisotropic materials and molecules.

Single-walled carbon nanotubes (SWNTs), rolled up from a single layer graphene into a cylinder, have excellent electrical, optical, mechanical, and thermal properties.[11] The various (*n*, *m*) indices of SWNT determine the diversity of the electronic structures. More importantly, the 1D feature of SWNT makes it a strictly anisotropic crystal, which provides an ideal model to systematically study the anisotropic charge interactions between molecules and the substrate in SERS. The Raman scattering of carbon nanotubes (CNTs) and molecules have been studied in the previous works based on the CNT bundles and composites of CNT and molecules.[11b,12] On the one hand, the CNTs in the bundles and composites were always not well aligned or oriented random. On the other hand, the Raman study on the CNT composites were always carried out by no consideration of polarized light or by the simple comparison of Raman spectra under parallel and cross polarization configurations.[11b,12] Systematic research on the polarization dependence of charger interaction between SWNTs and molecules was still absent. In this work, anisotropic Raman enhancement on horizontally aligned SWNT arrays was investigated. The Raman intensities of copper phthalocyanine (CuPc) and 3,4,9,10-perylene-tetracarboxylicacid-dianhydride (PTCDA) molecules adsorbed on SWNTs were enhanced by a factor of about 27 when the incident light polarization was parallel to the SWNTs and showed periodic variations with the sample rotation angle, indicating that the structural anisotropy of SWNT plays an important role in the angle-dependent Raman enhancement. This anisotropic Raman enhancement effect was attributed to the different pathways, and thus the different efficiency, of charge transfers when the laser polarization was parallel and perpendicular to the SWTNTs. Polarized optical absorption measurements also showed different redshifts and intensities of the probe molecules, further confirming the anisotropic charge transfer process. This work revealed the polarization and structure-dependent charge transfer interaction between molecules and anisotropic materials and provides a new path to study the chemical enhancement of SERS.

## 2. Results and Discussion

As illustrated in **Figure 1**a, the SWNT array was grown on $Al_2O_3$ and transferred onto a 300 nm $SiO_2$/Si or a glass substrate, followed by the deposition of CuPc molecules using vacuum thermal evaporation. As shown in Figure S1 in the Supporting Information, the Raman signals of CuPc molecules on SWNT array were enhanced about two times (depending on the vibrational modes) compared to that on the blank glass substrate under both 632.8 and 514.5 nm laser excitations. This Raman enhancement effect can be attributed to CM because no surface plasmon resonance can be excited in SWNT arrays using visible lasers. This Raman enhancement effect was an averaged result for all the SWNTs and all the molecules under the laser spot which was about 1 μm in diameter for the 100 × objective. For the SWNT array sample we used, the average diameter of SWNTs was about 1.5 nm, so only about 3.75% probe molecules were in direct contact with SWNTs for this sample (the density was about ≈25 SWNTs $\mu m^{-1}$). Therefore, the enhancement factor depended on the density of SWNT array, and the actual enhancement factor could be about ≈27 by taking into account of the estimated number of molecules adsorbed on SWNTs. The details for the calculation of actual enhancement factor were shown in Part S1 in the Supporting Information.

Raman spectra were collected under parallel polarization configuration (the polarization directions of incident light $e_i$ and collected scattering signal $e_s$ are parallel to each other) throughout this work unless otherwise stated. Red and green arrows in the incident light path representing in Figure 1a denote that $e_i$ parallel and perpendicular to SWNT axis direction, respectively. The polarized Raman spectra of CuPc molecules on SWNT array with 632.8 nm laser excitation are shown in Figure 1b. It can be seen that when $e_i$ was parallel to the SWNTs axis, the Raman signals of CuPc were stronger (about two to four times depending on the Raman modes) than that when they were perpendicular to each other. The Raman signals of CuPc molecules on the blank glass substrate remained

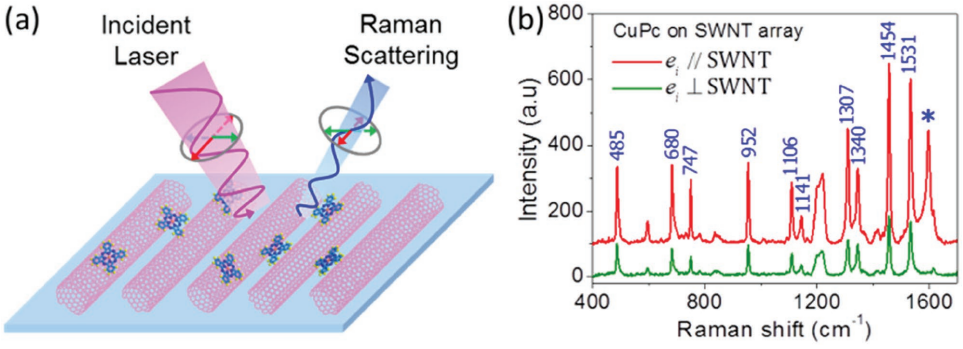


**Figure 1.** a) Schematic illustration of the anisotropic Raman scattering of CuPc molecules on single-walled carbon nanotube array. b) Polarized Raman spectra of CuPc molecules with SWNT array on bottom, where red and green lines are collected with incident laser polarized parallel to the SWNT axis direction under parallel polarization configuration. The "*" marked peak in (b) is the G band from SWNTs, and the excitation laser wavelength is 632.8 nm.

unchanged regardless of the angle between $e_i$ and the SWNT axis (Figure S3, Supporting Information). The anisotropic feature in the Raman signals of CuPc on SWNT array was not due to the interference effect of the substrate because the same can be observed on SWNT arrays on a transparent glass substrate. Hence, it is likely to originate from the interaction between CuPc molecules and SWNTs, demonstrating the important role of SWNT's strictly anisotropic characteristic in the Raman enhancement effect.

Angle-resolved polarized Raman spectroscopy (ARPRS), which has been used to study the crystalline orientation of anisotropic 2D layered materials,[13] was performed to systematically study the polarization dependence of the Raman enhancement effect of SWNT arrays. We define $\theta$ as the sample rotation angle, and $\theta_0$ refers to the initial angle $\theta$ before ARPRS measurements, which was usually fixed as 0° in this work. For the SWNT array sample shown in **Figure 2**a, the average density of about ≈40 SWNTs μm$^{-1}$ that could be estimated from the atomic force microscopy (AFM) and scanning electronic microscopy (SEM) images. It has been reported that the Raman modes of a single SWNT (radial breathing mode (RBM), G and G′ band) can only be detected when $e_i$ has a component polarized parallel to the SWNT axis, and the Raman intensity is proportional to $\cos^4(\theta + \theta_0)$ under parallel polarization configuration.[14] As shown in Figure 2b,d, the G band intensity of SWNTs was the maximum at $\theta$ = 0°/180° and was completely forbidden at $\theta$ = 90°, agreeing well with the previous work.[14a–d] It is interesting that Raman signals of CuPc molecules adsorbed on SWNTs showed the similar periodic variation with $\theta$, that is, the maximum intensities at $\theta$ = 0°/180° and the minimum at $\theta$ = 90°, as shown in Figure 2b. The nonzero minimum intensity at $\theta$ = 90° was mainly contributed by the molecules on the substrate. The polar plot of the peak intensity of 680 cm$^{-1}$ mode for CuPc with different $\theta$ is shown in Figure 2e, and the plots of other Raman peaks are shown in Figure S4 in the Supporting Information. Different from SWNT, the intensities of all Raman peaks for CuPc can be well fitted by $I = a + b\cos^2(\theta + \theta_0)$. However, the ratio between the maximum ($\theta$ = 0°/180°) and minimum ($\theta$ = 90°) intensities, which is defined as the degree of anisotropy (DOA = $(a + b)/a$) in this work, showed significant difference for different Raman peaks. From the fitting results, DOA was in the range of 4–10.

Similar to the enhancement factor, the DOA of CuPc molecules was closely related to the density of SWNT array. As shown in Figure S6 in the Supporting Information, the DOA of CuPc was decreased to about 2.5–6.0 for the SWNT array with density of about ≈32 SWNTs μm$^{-1}$, and it is about 2 for CuPc on SWNT array with density of about ≈12 SWNTs μm$^{-1}$, while almost no anisotropic features appear in the ARPRS of the sample with density of about ≈4 SWNTs μm$^{-1}$. It was important to point out that the actual DOA should be calculated by considering the CuPc molecules directly contacting with SWNTs. In order to estimate the actual DOA of CuPc on SWNT array, we put forward the following two assumptions: (1) the average diameter of SWNTs is about 1.5 nm, so only about 6% of the Raman signals we collected come from the CuPc molecules contacting with SWNTs for the sample in Figure 2a; (2) the Raman signals of CuPc for $\theta$ = 90° have the same intensities with that on blank substrate. Thus, the calculated DOA was in the range of 50–150. However, the Raman signals of CuPc on SWNT array were slightly decreased when $e_i$ is perpendicular to the SWNT axis direction. Therefore, the actual DOA should

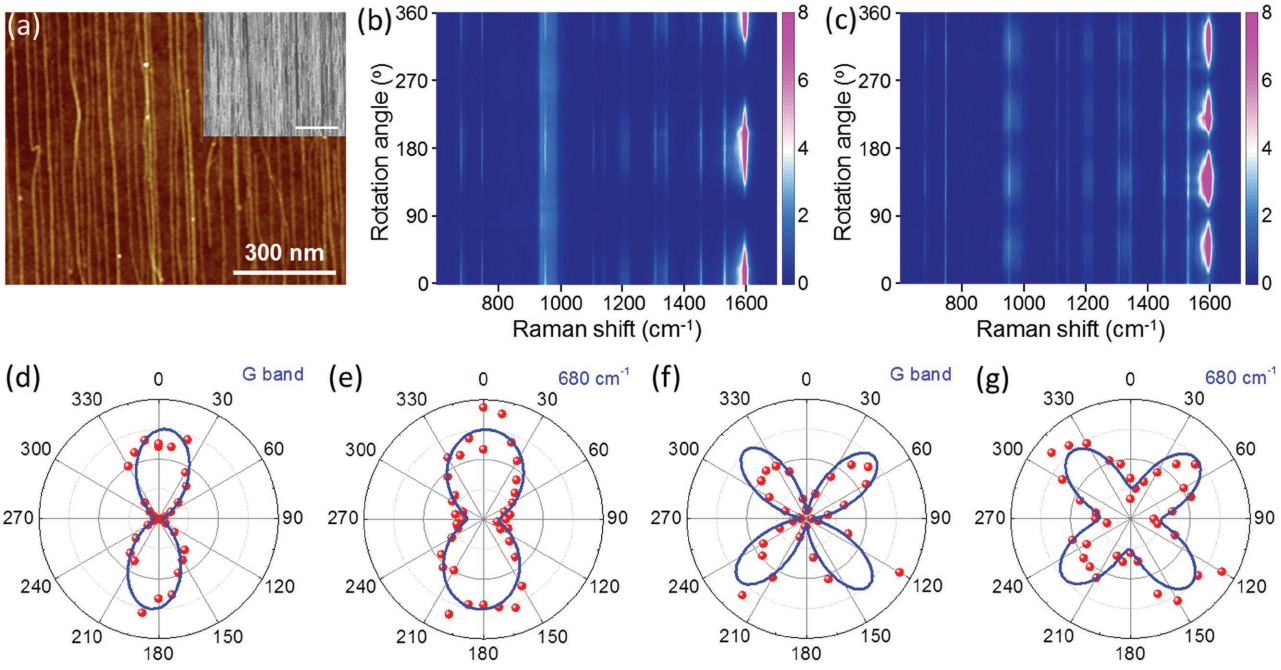


**Figure 2.** a) AFM image for a horizontally aligned SWNT array sample. Inset is the SEM image, and the scale bar is 2 μm. Angular dependence of polarized Raman spectra of CuPc molecules on SWNT array under b) parallel and c) crosspolarization configurations with 632.8 nm laser for excitation. Polar plots of the normalized intensities of d,f) G band for SWNT and e,g) 680 cm$^{-1}$ for CuPc molecules as a function of sample rotation angle under d,e) parallel and f,g) crosspolarization configurations.

be higher than 50 if all the Cu molecules were in direct contact with SWNTs (Part S3 in Supporting Information).

Under crosspolarization configuration (Figure 2c), both the Raman intensities of SWNTs and CuPc molecules exhibited 90° variation period with the sample rotation angle $\theta$, fitted by $I = c + d\cos^2(\theta + \theta_0)\sin^2(\theta + \theta_0)$,[14c] showing the minimum values at $\theta = 0°/90°$ and the maximum at $\theta = 45°$, as shown in Figure 2c,f,g. The difference was that G band from SWNT ($c = 0$) is completely forbidden at $\theta = 0°/90°$, while all the Raman modes of CuPc ($c \neq 0$) had nonzero intensities (Figure 2f,g and Figure S5, Supporting Information). Furthermore, the ratio between the maximum and minimum intensity also depended on the Raman modes. The strong correlation between the Raman signals of CuPc molecules and STNWs suggested the charge interactions between CuPc and SWNT, and the strict anisotropic characteristic of SWNT played an important role in the anisotropic Raman enhancement effect of SWNT arrays.

In order to study the influence of molecular resonance in the anisotropic Raman enhancement effect of SWNT arrays, we investigate ARPRS of CuPc molecules in SWNT arrays using excitation laser that is away from the absorption band of CuPc. The UV–vis absorption spectrum of CuPc on glass substrate is shown in **Figure 3**a. Two absorption bands were observed, that is, the Soret (B) band (transitions from HOMO − 1 and HOMO − 2 toward LUMO) in the region of 200–400 nm and the Q band ($\pi$–$\pi^*$ transition between HOMO and LUMO) in the region of 550–750 nm.[1d,15] Therefore, we chose the laser wavelength of 514.5 nm (2.41 eV) for excitation. In this case, only a few Raman peaks can be detected due to the nonresonant Raman scattering process of CuPc. Similarly, the Raman intensity (Figure 3c and Figure S7, Supporting Information) also showed 180° variation period with $\theta$ under nonresonant excitation, and DOA was in the region of 1.5–2.0 for 680, 1454, and 1531 $cm^{-1}$ modes and about 3.3 for the 1340 $cm^{-1}$ mode (may overlap with D band from SWNTs) for this sample. For comparison, the DOA was 2–4 for the resonant excitation using 632.8 nm laser line (Figure 3d and Figure S7, Supporting Information), which is larger than that under nonresonant condition. Take the 1454 $cm^{-1}$ phonon mode ($B_{2g}$, deformation of the isoindole ring system)[1d] as an example: DOA was 1.76 under 514.5 nm laser excitation, while it was 3.31 under 632.8 nm laser excitation.

To further clearly understand the influence of the electronic transitions in molecules on the anisotropic Raman-enhancement effect of SWNT arrays, we also chose PTCDA as a probe molecule, which shows strong absorption between 400 and 600 nm and is in resonance at 514.5 nm (Figure 3b). Similar to CuPc, the Raman signals of PTCDA on SWNT array were stronger than that on the blank glass substrate under 514.5 nm laser excitation, and the enhancement factor was in the range of 1.6–3.0 (Figure S2, Supporting Information). As shown in Figure 3e,f and Figure S8 in the Supporting Information, the ARPRS results of PTCDA molecules also showed periodic patterns; however, DOA was again much larger when the laser wavelength was 632.8 nm (DOA > 6) than that with excitation of 514.5 nm laser line (DOA = 2–3). This indicates that DOA of CuPc and PTCDA molecules on SWNT arrays was not mainly determined by the resonant electronic transitions in

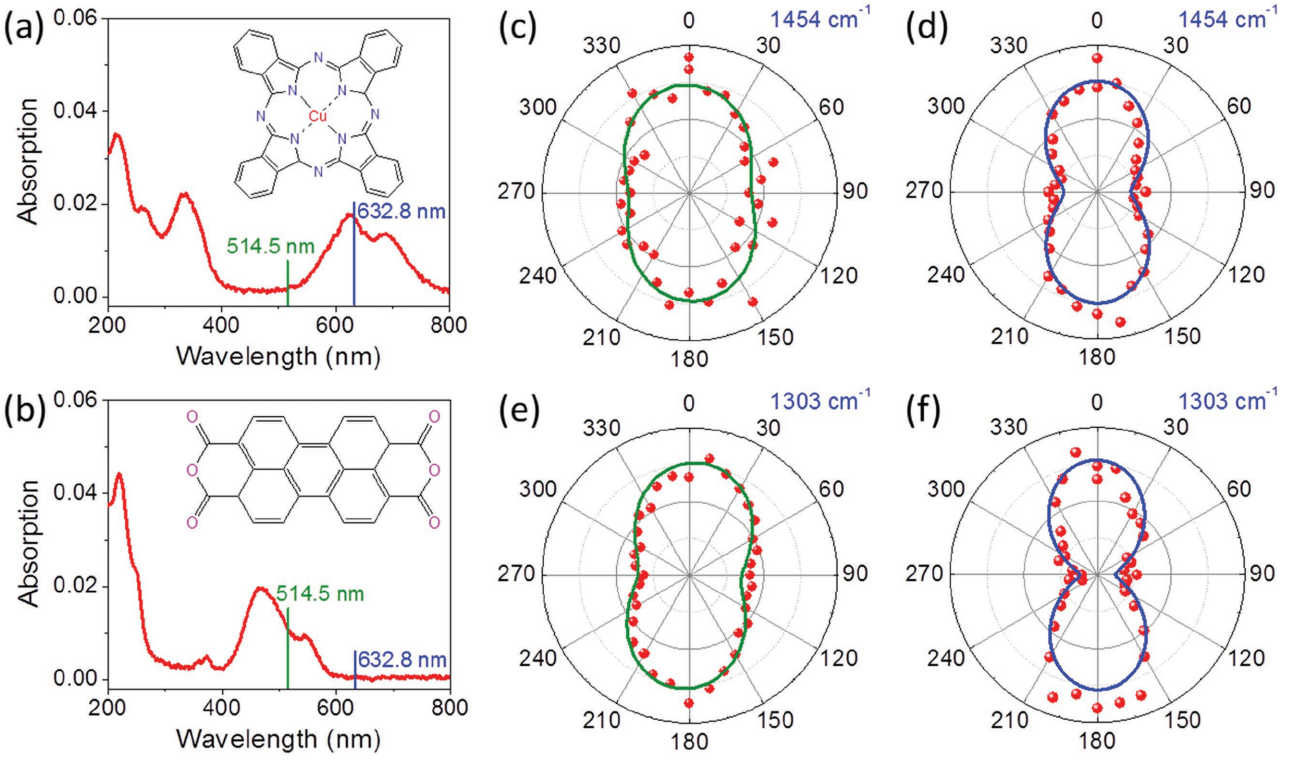


**Figure 3.** Absorption spectra of a) CuPc and b) PTCDA molecules. Green and blue lines are the laser wavelength for ARPRS measurements and insets are the corresponding molecular structures. Profiles for the intensities of c,d) 1454 $cm^{-1}$ mode of CuPc molecules and e,f) 1303 $cm^{-1}$ mode of PTCDA molecules at different sample rotation angles with c,e) 514.5 nm and d,f) 632.8 nm laser wavelength excitation.

the molecules, but rather by the excitation laser wavelength, or in other words, on other electronic resonances. Earlier studies have showed that parallel-connected conjugated ring of PTCDA could cause the relatively smaller PTCDA-graphene distance, and thus stretching the coupling between PTCDA and graphene, which could contribute to a larger GERS enhancement factor compared to CuPc.[4] Therefore, in comparison with CuPc, the larger DOA for PTCDA under both 514.5 and 632.8 nm laser excitations (the densities of SWNT arrays were all about ≈20 SWNT $\mu m^{-1}$ for these two samples) could be possibly attributed to the stronger PTCDA-SWNT coupling.

According to the group theory analysis, for a single CuPc molecule or a set of uniformly aligned molecules, the Raman scattering efficiency of the $B_{1g}$ and $B_{2g}$ modes have a 90° variation period with $\theta$ but with a 45° phase difference between the maximum intensities, while the $A_{1g}$ mode shows no polarization dependence (Figure S9, Supporting Information). In our experiments, the CuPc molecules were thermal deposited on the substrate with random orientations, so the Raman signals had no polarization dependence (Figure S3, Supporting Information), which has also been studied in the previous work in our group.[8] The AFM images of SWNTs before and after thermal evaporation of CuPc molecules illustrated the uniform distribution of molecules on SWNTs and the blank substrate, and the statistical diameter change of 30 SWNTs was in the range of 0.4–0.8 nm (Figure S10, Supporting Information), further indicating that there was no enrichment of molecules on SWNTs considering the measurement error.

Since aligned carbon nanotubes have been applied in photodetectors based on its anisotropic interaction with linearly polarized light,[16] in order to exclude the optical modulation effect of SWNTs on the polarization state of the incident and scattering light, we first exfoliated a few layer $MoS_2$ sheet on the SWNT array sample prior to the evaporation of organic molecules. As shown in Figure S11 in the Supporting Information, the anisotropic Raman signals no longer appeared in the ARPRS results, suggesting that the direct contact between SWNTs and molecules played an important role. These results implied that the anisotropic Raman enhancement of molecules on SWNTs array should be originated from the charge transfer between molecules and SWNTs.

In-plane anisotropic 2D layered materials exhibit the crystalline-orientation-dependent electronic properties, and thus the charge interactions between these materials and molecules are also possible to be crystalline-orientation dependent, leading to anisotropic Raman enhancement effect.[8] SWNT can be regarded as a cylinder rolled up from a single layer graphene, and possesses strict structural anisotropy. It is plausible that anisotropic charge interaction, especially anisotropic charge transfer, is responsible for the angle-dependent Raman enhancement effect of SWNT arrays. Theoretical studies suggested that exciton resonance in semiconductors can cause SERS enhancement.[5] Besides, Raman signals of CuPc on SWNTs in resonance with the incident laser were enhanced by about 10%–30% in magnitude compared to that on nonresonant SWNTs (Figure S12, Supporting Information). Therefore, we analyzed the energy alignment between CuPc and SWNTs which are in resonance with the incident laser energies (514.5 or 632.8 nm) and the schematic is shown in **Figure 4**a,b. Based on Fermi's golden rule, the electron transition probability per time can be expressed as[1b,6b]

$$w_{lk} = \frac{2\pi}{\hbar} g(E_k) \left| H'_{kl} \right|^2 \quad (1)$$

where $g(E_k)$ is the density of final states (DOS), and $H'_{kl}$ is the matrix element of perturbation between initial and final states. Under excitation of 632.8 nm laser, when $e_i$ is along to the SWNT axis, the electrons in the valence subband of SWNT can be excited to the conduction subband with the same index. Part of the excited electrons, instead of radiative damped or dissipating energy through heat, is allowed to transfer to the HOMO of CuPc, increasing the available DOS at the HOMO level and consequently the probability of electrons in the ground state being excited in the Raman scattering process of CuPc molecules. Since the absorption cross-section of SWNTs is much larger than molecules,[17] the DOS at the HOMO level of CuPc is expected to be significantly increased, leading to the Raman enhancement. However, when $e_i$ is perpendicular to the SWNT axis, the interband electronic transitions in SWNT are suppressed by the depolarization effect.[14g,18] In this case, the charge transfer could occur from the LUMO of CuPc to the conduction subband of SWNTs, reducing the available DOS in

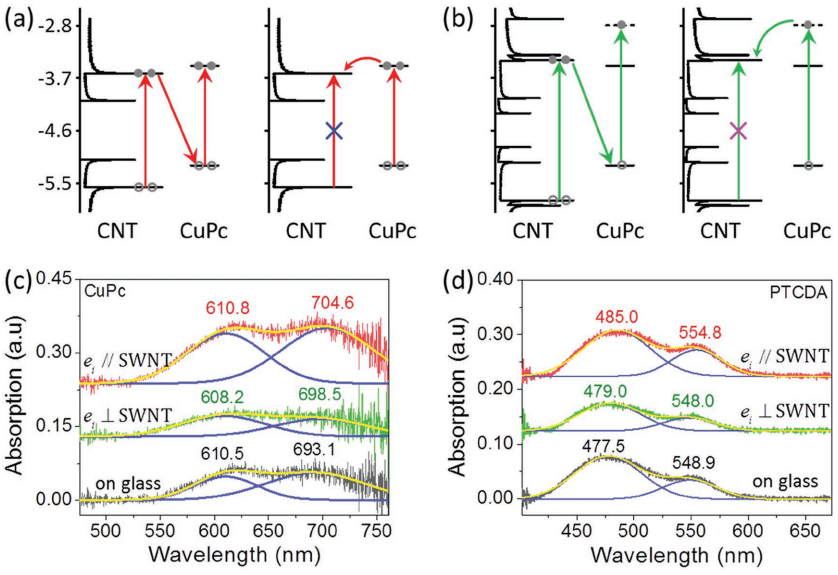


**Figure 4.** The schematic of energy alignment between SWNT and CuPc molecule, and the charge transfer under a) 632.8 nm and b) 514.5 nm excitation with laser polarized parallel (left) and perpendicular (right) to the SWNT. Polarized absorption spectra of c) CuPc and d) PTCDA molecules on SWNT array (red and green lines) and glass substrate (black lines) with incident light polarized parallel (red and black lines) and perpendicular (green lines) to the SWNT. The blue solid lines are fitting peaks using Gaussian functions, and the yellow solid lines are the sum of the fitting curves.

the excited state that contribute to the Raman scattering, so that the Raman signals of CuPc were slightly decreased (Figure S13, Supporting Information). The scenario is similar for the excitation wavelength of 514.5 nm (Figure S13, Supporting Information). Since the electrons can only be excited to a virtual energy level with excitation of 514.5 nm laser line, the charge transfer probability from CuPc to SWNT when $e_i$ is perpendicular to SWNT axis is smaller than that with 632.8 nm laser, which leads to a smaller reduction of Raman signals of CuPc. Combination with the comparable enhancement factor for $e_i$//SWNT, a weaker DOA was observed for 514.5 nm laser excitation.

This analysis is further supported by the polarized microabsorption spectra of the CuPc molecules on the SWNT arrays. Figure 4c shows the polarized absorption spectra of CuPc molecule on glass substrate with and without SWNT array. For CuPc deposited on a blank glass substrate, the absorption spectra showed no dependence on the incident polarization. The Q1 absorption band at ≈610.5 nm is attributed to the aggregated species due to the face-to-face stacking of CuPc molecule, and the Q2 band at ≈693.1 nm is assigned to the monomers of CuPc molecule.[11a] However, the absorption peak position and intensity of CuPc molecule on SWNT array were obviously different from that on blank substrate. Monomeric CuPc absorption (Q2 band) on SWNT array shows obvious redshift comparing to that on blank substrate, indicating the charge transfer interaction between CuPc and SWNTs. When $e_i$ is parallel to SWNT axis direction, the obvious absorption of SWNTs and charge transfer from SWNT to CuPc led to the increase of available DOS in HOMO of CuPc, and thus the enhanced absorption of CuPc, as shown in Figure 4c. When $e_i$ and SWNT axis were perpendicular to each other, no absorption of SWNTs and charge transfer from CuPc to SWNT could induce the slightly weakened absorption of CuPc. In other words, the electron transition probability of CuPc molecules showed polarization dependence when they were deposited on SWNT array, which was consistent to the angle-dependent Raman spectra of CuPc on SWNT arrays. Moreover, similar phenomenon can be observed in the polarized absorption spectra of PTCDA, as shown in Figure 4d. Redshift of absorption band and polarization-dependent absorption intensity demonstrated the anisotropic electron transition probability of PTCDA on SWNT, and then anisotropic Raman signals could be detected.

In our samples, SWNTs have different ($n$, $m$) index and thus different electronic energy bands. The charge transfer can only occur for a few SWNTs with the specific electronic band structures under laser excitation, that is, not all the SWNT can contribute to the Raman enhancement effect. At the same time, the diversity of chirality and electronic structure make it possible to investigate the complex charge interaction between probe molecules and SWNTs. Therefore, it is necessary to study the chirality-dependent Raman enhancement effect of SWNTs, and the anisotropic Raman enhancement effect on individual SWNT should be further studied using the SWNT sample with different chirality in detail.

## 3. Conclusion

In this work, the anisotropic Raman enhancement effect of SWNT was investigated using ARPRS. Anisotropic Raman signals of probe molecules (CuPc and PTCDA) deposited on SWNTs arrays were observed. Compared to the molecules on a blank substrate, the Raman intensities of molecules were enhanced by a factor of 1.5–4.0 when $e_i$ was parallel to the SWNT axis, while the Raman signals were slightly decreased when $e_i$ was perpendicular to the SWNTs axis. The model of energy band alignment between SWNTs and molecules was analyzed, and the polarization-dependent charge transfer was proposed to account for the anisotropic Raman enhancement. The analysis was further confirmed by polarized optical absorption measurements. The present work offers a new perspective for the exploration of complex charge interactions between SWNTs and organic molecules.

## 4. Experimental Section

*The Preparation of Sample*: SWNT arrays were grown on the $Al_2O_3$ substrate by using the chemical vapor deposition method similar to that previously reported in our group[19] and transferred onto $SiO_2$/Si (300 nm) or glass (1 mm) substrates using the polymethyl methacrylate (PMMA)-mediated transfer technique. The morphology and density of SWNT array were characterized by SEM and AFM. CuPc and PTCDA molecules were deposited on the SWNT arrays and quartz (500 μm) substrates through vacuum thermal evaporation, and the deposition thickness was controlled to be 3–5 Å, which should result in a submonolayer with random orientation.

*Polarized Raman Measurement*: Raman spectra were collected on a JY Horiba HR800 Raman system with 632.8 and 514.5 nm laser lines, and the laser power on the samples was kept below 0.5 mW for CuPc and 100 μW for PTCDA molecules to avoid laser-induced damage and photobleaching. Raman signals were collected using a Leica 100 × objective (numerical aperture NA = 0.90) and 600 lines $mm^{-1}$ grating (spectral resolution was about ≈1 $cm^{-1}$). To collect the polarized Raman spectra, a polarizer (polarizer I) was placed in the incident laser path and a polarization analyzer (polarizer II) was placed between the edge filter and the detector. Parallel polarization configuration was obtained when polarizers I and II were both along to the *Y*-axis, and crosspolarization configuration was achieved by placing a half-wave plate behind polarizer I to rotate the incident laser polarization direction with 90°. For the ARPRS measurements, a custom-built rotational stage, which has an accuracy of 1°, was used to continuously rotate the sample from 0° to 360° with a step of 10°. The Raman peaks were fitted with Lorentzian function, and the intensity of Raman peaks were determined by the peak area, that is, the field under the curve. The position of Raman peaks was calibrated by the 520 $cm^{-1}$ peak from the silicon substrate.

*The Measurement of Polarized Absorption*: The UV–vis absorption spectra of CuPc and PTCDA molecules on quartz substrate were performed on a Perkin-Elmer Lambda-950 UV/vis/near-IR spectrophotometer in the transmission mode. The polarized absorption spectra were carried out in confocal reflection mode on a Witec Alpha300RSA+ Raman system with a tungsten halogen light source. A Zeiss 50 × (NA = 0.75) objective was used to focus the incident light on the sample, and the reflected signal was collected and analyzed using a 300 lines $mm^{-1}$ grating spectrometer.

## Supporting Information

Supporting Information is available from the Wiley Online Library or from the author.

## Acknowledgements

This work was supported by the National Natural Science Foundation of China (NSFC) (Grant Nos. 21233001, 21790052, 51720105003,

 

11374355, and 21573004), the Ministry of Science and Technology (MOST) (Grant Nos. 2016YFA0200101, 2016YFA0200104, and 2015CB932400), the Beijing Municipal Science and Technology Planning Project (No. Z161100002116026), and the China Postdoctoral Science Foundation (2015M580010).

## Conflict of Interest

The authors declare no conflict of interest.

## Keywords

angle-resolved polarized Raman spectroscopy, anisotropic charge transfers, Raman-enhancements, single-walled carbon nanotubes

Received: August 2, 2017
Revised: September 26, 2017
Published online: December 1, 2017

[1] a) X. Ling, L. M. Xie, Y. Fang, H. Xu, H. L. Zhang, J. Kong, M. S. Dresselhaus, J. Zhang, Z. F. Liu, *Nano Lett.* **2010**, *10*, 553; b) X. Ling, W. J. Fang, Y. H. Lee, P. T. Araujo, X. Zhang, J. F. Rodriguez-Nieva, Y. X. Lin, J. Zhang, J. Kong, M. S. Dresselhaus, *Nano Lett.* **2014**, *14*, 3033; c) X. Ling, S. X. Huang, S. B. Deng, N. N. Mao, J. Kong, M. S. Dresselhaus, J. Zhang, *Acc. Chem. Res.* **2015**, *48*, 1862; d) X. Ling, J. X. Wu, W. G. Xu, J. Zhang, *Small* **2012**, *8*, 1365; e) S. Huh, J. Park, Y. S. Kim, K. S. Kim, B. H. Hong, J. M. Nam, *ACS Nano* **2011**, *5*, 9799; f) K. P. Loh, Q. L. Bao, G. Eda, M. Chhowalla, *Nat. Chem.* **2010**, *2*, 1015.

[2] X. Ling, J. Zhang, *Small* **2010**, *6*, 2020.

[3] a) H. Xu, L. M. Xie, H. L. Zhang, J. Zhang, *ACS Nano* **2011**, *5*, 5338; b) E. B. Barros, M. S. Dresselhaus, *Phys. Rev. B* **2014**, *90*, 035443.

[4] S. X. Huang, X. Ling, L. B. Liang, Y. Song, W. J. Fang, J. Zhang, J. Kong, V. Meunier, M. S. Dresselhaus, *Nano Lett.* **2015**, *15*, 2892.

[5] J. R. Lombardi, R. L. Birke, *J. Phys. Chem. C* **2014**, *118*, 11120.

[6] a) C. Muehlethaler, C. R. Considine, V. Menon, W. C. Lin, Y. H. Lee, J. R. Lombardi, *ACS Photonics* **2016**, *3*, 1164; b) Y. Yin, P. Miao, Y. M. Zhang, J. C. Han, X. H. Zhang, Y. Gong, L. Gu, C. Y. Xu, T. Yao, P. Xu, Y. Wang, B Song, S. Jin, *Adv. Funct. Mater.* **2017**, *27*, 1606694.

[7] Y. Tan, L. N. Ma, Z. B. Gao, M. Chen, F. Chen, *Nano Lett.* **2017**, *17*, 2621.

[8] J. J. Lin, L. B. Liang, X. Ling, S. Q. Zhang, N. N. Mao, N. Zhang, B. G. Sumpter, V. Meunier, L. M. Tong, J. Zhang, *J. Am. Chem. Soc.* **2015**, *137*, 15511.

[9] a) R. Livingstone, X. C. Zhou, M. C. Tamargo, J. R. Lombardi, L. C. Quagliano, F. Jean-Mary, *J. Phys. Chem. C* **2010**, *114*, 17460; b) Z. Liu, H. M. Zhu, N. H. Song, T. Q. Lian, *Nano Lett.* **2013**, *13*, 5563; c) I. Alessandri, J. R. Lombardi, *Chem. Rev.* **2016**, *116*, 14921.

[10] N. N. Mao, J. X. Wu, B. W. Han, J. J. Lin, L. M. Tong, J. Zhang, *Small* **2016**, *12*, 2627.

[11] a) M. Y. Sfeir, F. Wang, L. M. Huang, C. C. Chuang, J. Hone, S. P. O'Brien, T. F. Heinz, L. E. Brus, *Science* **2004**, *306*, 1540; b) A. M. Rao, P. C. Eklund, S. Bandow, A. Thess, R. E. Smalley, *Nature* **1997**, *388*, 257; c) Y. B. Chen, J. Zhang, *Acc. Chem. Res.* **2014**, *47*, 2273.

[12] a) M. J. O'Connell, E. E. Eibergen, S. K. Doorn, *Nat. Mater.* **2005**, *4*, 412; b) J. Y. Ji, G. Sui, Y. H. Yu, Y. X. Liu, Y. H. Lin, Z. J. Du, S. Ryu, X. P. Yang, *J. Phys. Chem. C* **2009**, *113*, 4779.

[13] J. X. Wu, N. N. Mao, L. M. Xie, H. Xu, J. Zhang, *Angew. Chem., Int. Ed.* **2015**, *54*, 2366.

[14] a) M. F. Islam, D. E. Milkie, C. L. Kane, A. G. Yodh, J. M. Kikkawa, *Phys. Rev. Lett.* **2004**, *93*, 037404; b) G. S. Duesberg, I. Loa, M. Burghard, K. Syassen, S. Roth, *Phys. Rev. Lett.* **2000**, *85*, 5436; c) A. Jorio, A. G. Souza, V. W. Brar, A. K. Swan, M. S. Ünlü, B. B. Goldberg, A. Righi, J. H. Hafner, C. M. Lieber, R. Saito, G. Dresselhaus, M. S. Dresselhaus, *Phys. Rev. B* **2002**, *65*, 121402; d) A. Jorio, M. A. Pimenta, A. G. Souza, G. G. Samsonidze, A. K. Swan, M. S. Unlu, B. B. Goldberg, R. Saito, G. Dresselhaus, M. S. Dresselhaus, *Phys. Rev. Lett.* **2003**, *90*, 107403; e) A. Jorio, G. Dresselhaus, M. S. Dresselhaus, M. Souza, M. S. S. Dantas, M. A. Pimenta, A. M. Rao, R. Saito, C. Liu, H. M. Cheng, *Phys. Rev. Lett.* **2000**, *85*, 2617; f) A. M. Rao, A. Jorio, M. A. Pimenta, M. S. S. Dantas, R. Saito, G. Dresselhaus, M. S. Dresselhaus, *Phys. Rev. Lett.* **2000**, *84*, 1820; g) M. S. Dresselhaus, G. Dresselhaus, R. Saito, A. Jorio, *Phys. Rep.* **2005**, *409*, 47.

[15] E. Salomon, N. Papageorgiou, Y. Ferro, J. M. Layet, *Thin Solid Films* **2004**, *466*, 259.

[16] L. Zhang, Y. Wu, L. Deng, Y. Zhou, C. H. Liu, S. S. Fan, *Nano Lett.* **2016**, *16*, 6378.

[17] a) E. Blanco, D. N. Rao, F. J. Aranda, D. V. G. L. N. Rao, S. Tripathy, J. A. Akkara, R. Litran, M. Ramirez-del-Solar, *J. Appl. Phys.* **1998**, *83*, 3441; b) S. R. Sanchez, S. M. Bachilo, Y. Kadria-Vili, C. W. Lin, R. B. Weisman, *Nano Lett.* **2016**, *16*, 6903.

[18] G. G. Samsonidze, R. Saito, A. Jorio, M. A. Pimenta, A. G. Souza, A. Gruneis, G. Dresselhaus, M. S. Dresselhaus, *J. Nanosci. Nanotechnol.* **2003**, *3*, 431.

[19] Y. Hu, L. X. Kang, Q. C. Zhao, H. Zhong, S. C. Zhang, L. W. Yang, Z. Q. Wang, J. J. Lin, Q. W. Li, Z. Y. Zhang, L. M. Peng, Z. F. Liu, J. Zhang, *Nat. Commun.* **2014**, *6*, 6099.

 